Mikada, H., Moore, G.F., Taira, A., Becker, K., Moore, J.C., and Klaus, A. (Eds.)
Proceedings of the Ocean Drilling Program, Scientific Results Volume 190/196

19. Data Report: Initial Permeability Determinations on Sediments from the Nankai Trough Accretionary Prism, ODP Sites 1173 and 1174[1]

R.H. Adatia[2] and A.J. Maltman[2]

ABSTRACT

Understanding the role of fluids in active accretionary prisms requires quantitative knowledge of parameters such as permeability. We report here the results of permeability tests on four samples from Ocean Drilling Program Leg 190 at the Nankai Trough accretionary prism—two from Site 1173 and two from Site 1174. Volcanic ash is present in one of the samples; otherwise, the material is hemipelagic mud. A constant-rate-of-flow technique was used at various effective pressures and rates of flow. The permeability of the four samples ranges between 10^{-15} and 10^{-18} m^2, with the ash-bearing sample showing the highest values.

INTRODUCTION

The Nankai Trough accretionary prism off the southwest coast of Japan is an instructive area for understanding the relationship between deformation, diagenesis, and hydrogeology. Here, the Shikoku Basin, developed on the Philippine Sea plate, is subducting beneath the Eurasian plate with active accretion of sediment. The analysis of cores from the area where deformation and the décollement are initiated is an important approach to understanding the role of fluids in the processes at the prism toe and the initiation of its basal décollement. During Ocean Drilling Program (ODP) Leg 190, the Nankai Prism was cored at several sites, including an undeformed reference site (Site 1173) oceanward of

[1] Adatia, R.H., and Maltman, A.J., 2004. Data report: Initial permeability determinations on sediments from the Nankai Trough accretionary prism, ODP Sites 1173 and 1174. *In* Mikada, H., Moore, G.F., Taira, A., Becker, K., Moore, J.C., and Klaus, A. (Eds.), *Proc. ODP, Sci. Results,* 190/196, 1–12 [Online]. Available from World Wide Web: <http://www-odp.tamu.edu/publications/190196SR/VOLUME/CHAPTERS/214.PDF>. [Cited YYYY-MM-DD]
[2] Institute of Geography and Earth Sciences, University of Wales, Aberystwyth, Llandinum Building, Aberystwyth SY23 3DB, Wales, United Kingdom. Correspondence author: **rha00@aber.ac.uk**

Initial receipt: 21 November 2002
Acceptance: 22 August 2003
Web publication: 12 April 2004
Ms 190SR-214

the prism and a site (Site 1174) of proto-thrusting and incipient development of the basal décollement (Moore et al., 2001; Shipboard Scientific Party, 2001). Knowledge of permeability is fundamental to an understanding of the hydrogeological behavior of cored material. Preliminary laboratory measurements were conducted on two samples each from Sites 1173 and 1174 and are reported here. A constant-rate-of-flow technique was implemented using the triaxial cell system outlined in Figure F1. Permeability testing on additional samples from Sites 1174–1178 is currently in progress.

F1. Permeability flow pump method, p. 6.

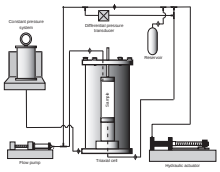

T1. Overview of samples tested, p. 8.

METHODS/MATERIALS

During ODP Leg 190, whole-round samples were collected by the Shipboard Scientific Party of the *JOIDES Resolution*. The samples were cut from the cores after routine testing for physical properties but before splitting. They were then encased and wax-sealed while still in the core liner for transportation and subsequent storage. The whole-round cores were maintained under continuous refrigeration at 5°C until testing. The four samples tested (190-1173A-13H-4, 86–101 cm, 18H-6, 20–40 cm, 190-1174B-27R-3, 120–137 cm, and 33R-4, 20–35 cm) are primarily hemipelagic muds, with ash laminations in Sample 190-1173A-18H-6, 20–40 cm (Table T1). These four samples were selected to represent undeformed sediments at the two sites.

The flow-pump technique has a number of advantages over the more traditional falling-head and constant-head techniques for the measurement of permeabilities of fine-grained and marine sediments (i.e., Olsen et al., 1985; Morin and Olsen, 1987; Aiban and Znidarcic, 1989). Advantages include increased accuracy due to the electronically controlled flow rate and automated data recovery, a constant-head difference at steady-state conditions that minimizes damage to samples caused by excessive gradients, and reduction of consolidation induced by seepage. Also, the absence of a fluid/air interface minimizes air in the system and back pressure helps to ensure dissolution of small air bubbles and saturation.

Prior to testing, each sample was cut to a 38 mm × 76 mm cylinder. The trimmed sample was encased within a latex sleeve, capped at both ends with filter paper and a porous disk, and then saturated with deaired water. The samples were confined by pressurized deionized water within a triaxial cell. An infusion flow pump and digital hydraulic actuator, linked by a differential pressure transducer, controlled input and output of permeant to the sample within the triaxial cell. All aspects of the system were computer linked, and measurements and data logs were automated. Deionized, deaired water was used as permeant to prevent corrosion. A permeant with a chemistry designed to simulate natural porewater may help minimize the possibility of clay swelling and shrinkage (Stover et al., 2001), but the low rates of flow used here mean that the sample was exposed to little permeant other than its natural pore fluid.

The sample was saturated by the application of back pressure and the degree of saturation was assessed by employing the Skempton B-test. This involved systematically isolating the sample fluid while altering the confining pressures and monitoring the associated change in differential pressure. When a *B*-value of ~0.95 for the samples was obtained,

where

$$B = \Delta \text{ differential pressure}/\Delta \text{ cell pressure}$$

(Skempton, 1954), the sample was judged to be sufficiently saturated.

Bolton et al. (2000) noted significant variations in permeability at effective pressures <100 kPa and relatively little change at values >100 kPa (Kemerer and Screaton, 2001). Preliminary investigations during the present work suggest that differing rates of flow may also affect permeability; therefore, the present tests employed a range of effective pressures and flow rates. The effective pressures were increased incrementally; samples were tested only after reaching equilibrium at each increment, until there was no significant decrease in permeability. This procedure also helps ensure a reduction in the effects of rebound and other changes in the sample due to coring procedures and sample preparation. Back pressure was maintained at 350 kPa, and tests were carried out at a series of confining fluid pressures of 375 to 800 kPa. Effective pressures therefore ranged from 25 to 450 kPa. Effective pressures in situ would be much greater than effective pressures generated by the triaxial cell; therefore, maximum effective pressure values should be used.

Tests were conducted at various rates of flow for each confining fluid pressure, but the rate of flow in each individual test was kept constant. Samples were not deformed during testing. Because differences between hydraulic head at the points of permeant entry and exit can cause loss of energy and permeability fluctuations, head gradients were monitored for the presence of steady-state conditions to ensure equilibrium of pressure throughout the sample. Darcy's law was used to obtain hydraulic conductivity (K) using the equation

$$Q = -KA\,(\Delta h/\Delta l), \tag{1}$$

where

- Q = rate of flow (m^3/s),
- K = hydraulic conductivity (m/s),
- A = sample area (m^2) (calculated from sample diameter),
- Δh = head difference (m) (calculated from pressure difference across sample), and
- Δl = sample length (m),

and intrinsic permeability figures were derived from hydraulic conductivity values using the equation

$$K = K_i\,(\rho g/\mu), \tag{2}$$

where

- K = hydraulic conductivity (m/s),
- K_i = intrinsic permeability (m^2),
- μ = dynamic viscosity (0.001 Pa·s),
- ρ = water density (1000 kg/m^3), and
- g = acceleration of gravity (9.81 m/s^2).

The viscosity value for water at 20°C, the temperature at which all the tests were conducted, was used.

RESULTS

The full results are presented in the accompanying tables. In summary, the permeabilities of the four samples tested ranged from 10^{-15} to 10^{-18} m^2.

The permeability of Sample 190-1173A-13H-4, 86–101 cm, ranged from 10^{-16} to 10^{-17} m^2 at effective pressures of 50, 100, and 150 kPa (Table T2). The permeability of Sample 190-1173A-18H-6, 20–40 cm, ranged from 10^{-15} to 10^{-17} m^2 at effective pressures of 25, 50, 100, 150, and 200 kPa (Table T3). The permeability of Sample 190-1174B-27R-3, 120–137 cm, ranged from 10^{-16} to 10^{-18} m^2 at effective pressures of 50, 75, 100, and 150 kPa (Table T4). The permeability of Sample 190-1174B-33R-4, 20–35 cm, ranged from 10^{-16} to 10^{-18} m^2 at effective pressures of 50, 100, 150, 250, 350, and 450 kPa (Table T5).

Permeabilities measured at 25 kPa effective pressure (10^{-15} m^2) were one order of magnitude higher than those measured at 50 kPa. With increases of effective pressure up to 450 kPa, permeability decreased to a minimum of 10^{-18} m^2 (Fig. F2).

At an effective pressure of 150 kPa, the permeability of Samples 190-1173A-18H-6, 20–40 cm, 190-1174B-27R-3, 120–137 cm, and 190-1174B-33R-4, 20–35 cm, was 10^{-17} m^2 and that of Sample 190-1173A-18H-6, 20–40 cm, was 10^{-16} m^2.

None of the samples contain visible deformation structures. Overall, the sample tending to show the highest permeability, in some circumstances by two or three orders of magnitude, is 190-1173A-18H-6, 20–40 cm. This sample, which contains ash laminations, was taken from a section with abundant volcanic ash. The remaining samples, showing generally lower permeabilities, consist entirely of hemipelagic mud. These preliminary results therefore suggest that although varying effective pressures and flow rates have an effect on permeability, the primary control is lithology.

ACKNOWLEDGMENTS

This research used samples and/or data provided by the Ocean Drilling Program (ODP). ODP is sponsored by the U.S. National Science Foundation (NSF) and participating countries under management of Joint Oceanographic Institutions (JOI), Inc. Grateful acknowledgment is given to the crew of the *JOIDES Resolution* and the ODP Leg 190 scientific team. The authors would like to thank Andy Fisher and Brandon Dugan for reviewing the manuscript and providing helpful suggestions and comments. R.H.A. would also like to thank A.J. Bolton and B. Hubbard for advice and support and D. Kelly and G. Duller for computer assistance.

Funding was provided by the Natural Environment Research Council (NERC grant number NER/S/J/2000/05943) to R.H.A.

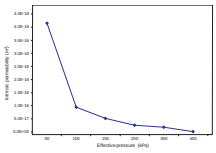

REFERENCES

Aiban, S.A., and Znidarcic, D., 1989. Evaluation of the flow pump and constant head techniques for permeability measurements. *Géotechnique,* 39:655–666.

Bolton, A., Maltman, A.J., and Fisher, Q., 2000. Anisotropic permeability and bimodal pore-size distributions of fine-grained marine sediments. *Mar. Pet. Geol.,* 17:657–672.

Kemerer, A., and Screaton, E., 2001. Permeabilities of sediments from Woodlark Basin: implications for pore pressures. *In* Huchon, P., Taylor, B., and Klaus, A. (Eds.), *Proc. ODP, Sci. Results,* 180, 1–14 [Online]. Available from World Wide Web: <http://www-odp.tamu.edu/publications/180_SR/VOLUME/CHAPTERS/169.PDF>. [Cited 2002-11-18]

Moore, G.F., Taira, A., Klaus, A., Becker, L., Boeckel, B., Cragg, A., Dean, A., Fergusson, C.L., Henry, P., Hirano, S., Hisamitsu, T., Hunze, S., Kastner, M., Maltman, A.J., Morgan, J.K., Murakami, Y., Saffer, D.M., Sánchez-Gómez, M., Screaton, E.J., Smith, D.C., Spivack, A.J., Steurer, J., Tobin, H.J., Ujiie, K., Underwood, M.B., and Wilson, M., 2001. New insights into deformation and fluid flow processes in the Nankai Trough accretionary prism: results of Ocean Drilling Program Leg 190. *Geochem. Geophys. Geosyst.,* 2:10.129/2001GC00166.

Morin, R.H., and Olsen, H.W., 1987. Theoretical analysis of the transient pressure response from a constant flow rate hydraulic conductivity test. *Water Resour. Res.,* 23:1461–1470.

Olsen, H.W., Nichols, R.W., and Rice, T.L., 1985. Low gradient permeability measurements in a triaxial system. *Géotechnique,* 35:145–157.

Shipboard Scientific Party, 2001. Leg 190 summary. *In* Moore, G.F., Taira, A., Klaus, A., et al., *Proc. ODP, Init. Repts.,* 190: College Station TX (Ocean Drilling Program), 1–87.

Skempton, A.W., 1954. The pore pressure coefficients A and B. *Geotechnique,* 4:4–143.

Stover, S.C., Screaton, E.J., Likos, W.J., and Ge, S., 2001. Data report: Hydrologic characteristics of shallow marine sediments of Woodlark Basin, Site 1109. *In* Huchon, P., Taylor, B., and Klaus, A. (Eds.), *Proc. ODP, Sci. Results,* 180, 1–22 [Online]. Available from World Wide Web: <http://www-odp.tamu.edu/publications/180_SR/VOLUME/CHAPTERS/168.PDF>. [Cited 2002-11-18]

Figure F1. Flow pump method of permeability testing.

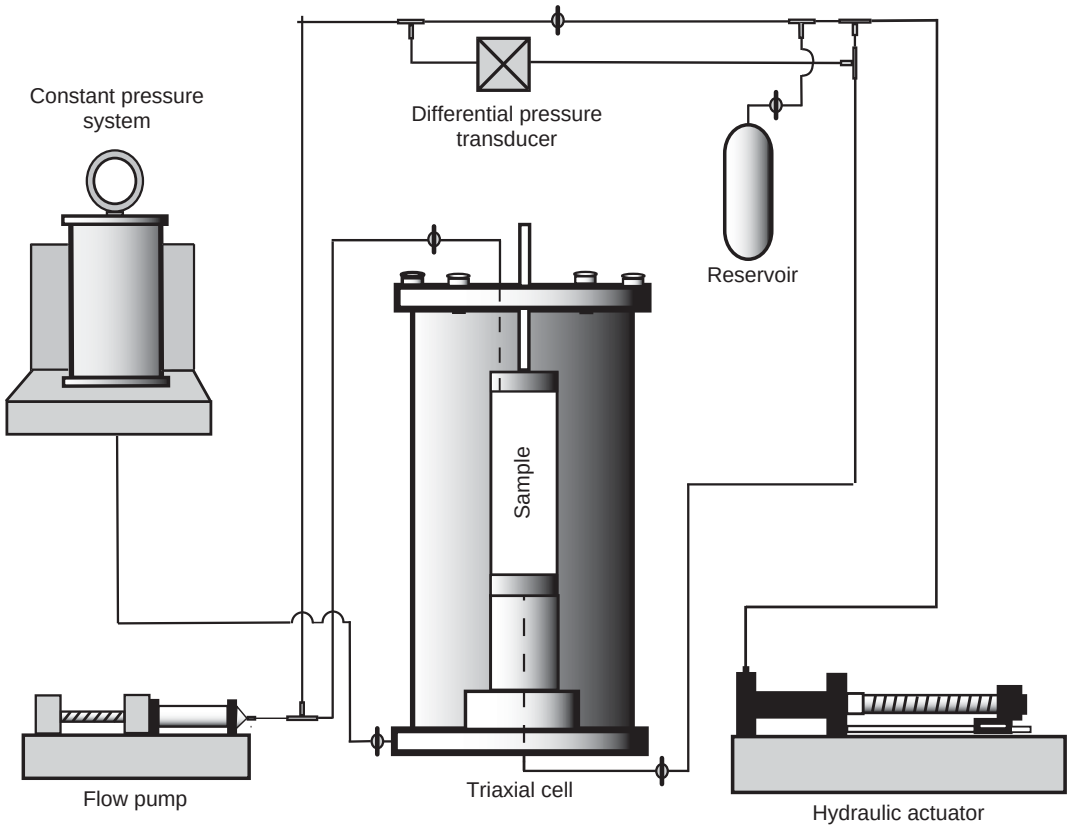

Figure F2. Decrease of permeability with increasing effective stress for Sample 190-1174B-33R-4, 20–35 cm (452.90 mbsf), trimmed at 21.5–29.1 cm.

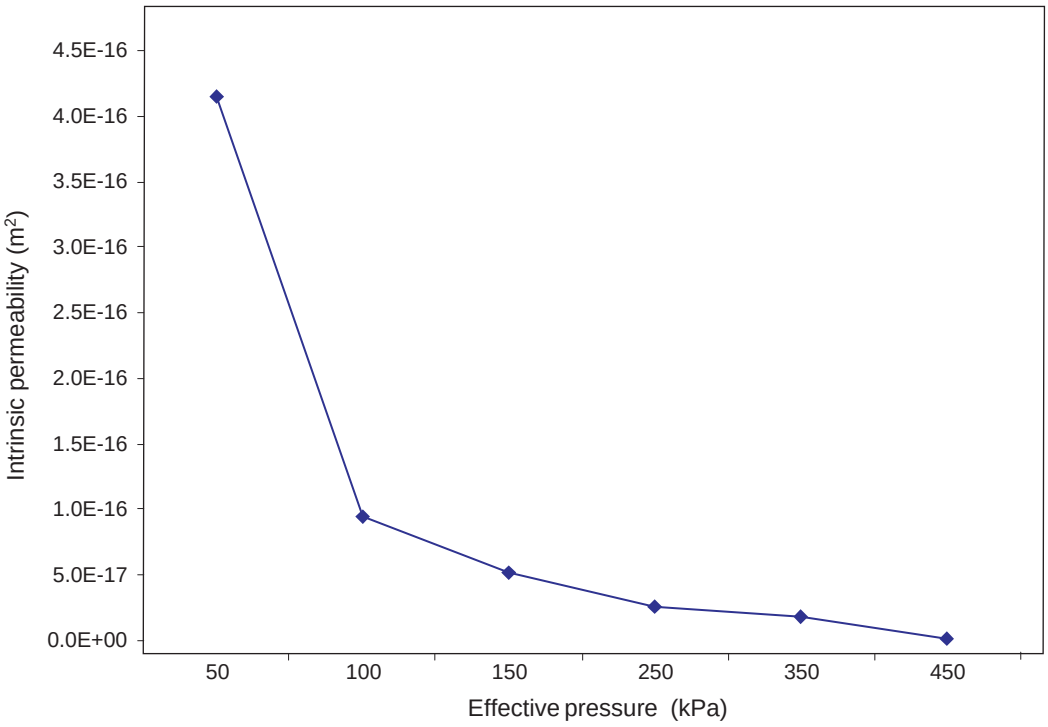

Table T1. Overview of samples tested.

Core, section, interval (cm)	Depth (mbsf)	Unit, subunit, and facies	Lithology of facies	Additional sample notes
190-1173A-				
13H-4, 86–101	117.00	Unit II: upper Shikoku Basin facies	Hemipelagic mud with abundant ash	Hemipelagic mud
18H-6, 20–40	166.84	Unit II: upper Shikoku Basin facies	Hemipelagic mud with abundant ash	Coarse and fine ash layers. Pink and white.
190-1174B-				
27R-3, 120–137	394.70	Unit IIB: outer trench-wedge facies	Silt turbidites, hemipelagic mud	Hemipelagic mud
33R-4, 20–35	452.90	Unit IIC: trench-to-basin transition facies	Silt turbidites, volcanic ash, hemipelagic mud	Hemipelagic mud

Table T2. Permeability test results for Sample 190-1173A-13H-4, 86–101 cm (117.00 mbsf), trimmed at 89.7–97.3 cm.

Sample and test number	Effective pressure (kPa)	Length (m)	Area (m^2)	Flow rate (mL/min)	Flow rate (m^3/s)	Fluid flux (m/s)	Differential pressure (kPa)	Head (m)	Head gradient (m)	Hydraulic conductivity (m/s)	Intrinsic permeability (m^2)
Nankaitest1	50	0.076	0.0011	0.005	8.33E–11	7.35E–08	14.00	1.43	18.78	3.91E–09	3.99E–16
Nankaitest2	100	0.076	0.0011	0.005	8.33E–11	7.35E–08	300.00	30.58	402.38	1.83E–10	1.86E–17
Nankaitest3	150	0.076	0.0011	0.005	8.33E–11	7.35E–08	232.00	23.65	311.18	2.36E–10	2.41E–17

Table T3. Permeability test results for Sample 190-1173A-18H-6, 20–40 cm (166.84 mbsf), trimmed at 31.1–38.7 cm.

Sample and test number	Effective pressure (kPa)	Length (m)	Area (m^2)	Flow rate (mL/min)	Flow rate (m^3/s)	Fluid flux (m/s)	Differential pressure (kPa)	Head (m)	Head gradient (m)	Hydraulic conductivity (m/s)	Intrinsic permeability (m^2)
73a18p37	200	0.076	0.0011	0.011	1.83E–10	1.62E–07	141.69	14.44	190.05	8.51E–10	8.68E–17
73a18p34	200	0.076	0.0011	0.031	5.17E–10	4.56E–07	184.19	18.78	247.05	1.84E–09	1.88E–16
73a18p35	200	0.076	0.0011	0.051	8.50E–10	7.49E–07	250.55	25.54	336.06	2.23E–09	2.27E–16
73a18p07	150	0.076	0.0011	0.001	1.67E–11	1.47E–08	2.61	0.27	3.50	4.20E–09	4.28E–16
73a18p08	150	0.076	0.0011	0.005	8.33E–11	7.35E–08	25.78	2.63	34.58	2.13E–09	2.17E–16
73a18p10	150	0.076	0.0011	0.011	1.83E–10	1.62E–07	58.84	6.00	78.92	2.05E–09	2.09E–16
73a18p14	150	0.076	0.0011	0.031	5.17E–10	4.56E–07	117.78	12.01	157.98	2.88E–09	2.94E–16
73a18p12	150	0.076	0.0011	0.041	6.83E–10	6.03E–07	139.14	14.18	186.62	3.23E–09	3.29E–16
73a18p11	150	0.076	0.0011	0.051	8.50E–10	7.49E–07	137.62	14.03	184.59	4.06E–09	4.14E–16
73a18p38	150	0.076	0.0011	0.071	1.18E–09	1.04E–06	176.34	17.98	236.52	4.41E–09	4.50E–16
73a18p21	100	0.076	0.0011	0.003	5.00E–11	4.41E–08	14.99	1.53	20.11	2.19E–09	2.24E–16
73a18p20	100	0.076	0.0011	0.005	8.33E–11	7.35E–08	22.40	2.28	30.04	2.45E–09	2.49E–16
73a18p22	100	0.076	0.0011	0.007	1.17E–10	1.03E–07	17.96	1.83	24.09	4.27E–09	4.36E–16
73a18p24	100	0.076	0.0011	0.008	1.33E–10	1.18E–07	48.68	4.96	65.29	1.80E–09	1.84E–16
73a18p23	100	0.076	0.0011	0.009	1.50E–10	1.32E–07	39.09	3.98	52.43	2.52E–09	2.57E–16
73a18p25	100	0.076	0.0011	0.011	1.83E–10	1.62E–07	63.39	6.46	85.02	1.90E–09	1.94E–16
73a18p26	100	0.076	0.0011	0.031	5.17E–10	4.56E–07	106.90	10.90	143.38	3.18E–09	3.24E–16
73a18p27	100	0.076	0.0011	0.051	8.50E–10	7.49E–07	123.42	12.58	165.54	4.53E–09	4.62E–16
73a18p19	50	0.076	0.0011	0.005	8.33E–11	7.35E–08	24.82	2.53	33.29	2.21E–09	2.25E–16
73a18p18	50	0.076	0.0011	0.006	1.00E–10	8.82E–08	43.11	4.39	57.82	1.52E–09	1.56E–16
73a18p17	50	0.076	0.0011	0.007	1.17E–10	1.03E–07	33.36	3.40	44.74	2.30E–09	2.35E–16
73a18p16	50	0.076	0.0011	0.008	1.33E–10	1.18E–07	47.28	4.82	63.42	1.85E–09	1.89E–16
73a18p15	50	0.076	0.0011	0.011	1.83E–10	1.62E–07	58.76	5.99	78.81	2.05E–09	2.09E–16
73a18p30	25	0.076	0.0011	0.011	1.83E–10	1.62E–07	53.77	5.48	72.12	2.24E–09	2.29E–16
73a18p29	25	0.076	0.0011	0.031	5.17E–10	4.56E–07	51.25	5.22	68.74	6.63E–09	6.76E–16
73a18p28	25	0.076	0.0011	0.051	8.50E–10	7.49E–07	41.37	4.22	55.49	1.35E–08	1.38E–15
73a18p31	25	0.076	0.0011	0.071	1.18E–09	1.04E–06	52.98	5.40	71.06	1.47E–08	1.50E–15
73a18p32	25	0.076	0.0011	0.091	1.52E–09	1.34E–06	55.86	5.69	74.92	1.78E–08	1.82E–15

Table T4. Permeability test results for Sample 190-1174B-27R-3, 120–137 cm (394.70 mbsf), trimmed at 122.4–130.0 cm.

Sample and test number	Effective pressure (kPa)	Length (m)	Area (m^2)	Flow rate (mL/min)	Flow rate (m^3/s)	Fluid flux (m/s)	Differential pressure (kPa)	Head (m)	Head gradient (m)	Hydraulic conductivity (m/s)	Intrinsic permeability (m^2)
74b27p11	150	0.076	0.0011	0.005	8.33E–11	7.35E–08	181.11	18.46	242.92	3.02E–10	3.09E–17
74b27p12	150	0.076	0.0011	0.011	1.83E–10	1.62E–07	182.32	18.59	244.55	6.61E–10	6.74E–17
74b27p13	150	0.076	0.0011	0.031	5.17E–10	4.56E–07	181.09	18.46	242.89	1.88E–09	1.91E–16
74b27p02	100	0.076	0.0011	0.001	1.67E–11	1.47E–08	114.67	11.69	153.81	9.55E–11	9.75E–18
74b27p03	100	0.076	0.0011	0.005	8.33E–11	7.35E–08	126.85	12.93	170.14	4.32E–10	4.41E–17
74b27p04	100	0.076	0.0011	0.011	1.83E–10	1.62E–07	126.76	12.92	170.02	9.51E–10	9.70E–17
74b27p05	100	0.076	0.0011	0.031	5.17E–10	4.56E–07	127.31	12.98	170.76	2.67E–09	2.72E–16
74b27p06	100	0.076	0.0011	0.051	8.50E–10	7.49E–07	122.66	12.50	164.52	4.56E–09	4.65E–16
74b27p07	100	0.076	0.0011	0.071	1.18E–09	1.04E–06	122.64	12.50	164.49	6.34E–09	6.47E–16
74b27p08	100	0.076	0.0011	0.091	1.52E–09	1.34E–06	122.45	12.48	164.24	8.14E–09	8.31E–16
74b27p29	75	0.076	0.0011	0.000511	8.52E–12	7.51E–09	197.49	20.13	264.89	2.83E–11	2.89E–18
74b27p24	50	0.076	0.0011	0.001	1.67E–11	1.47E–08	178.02	18.15	238.78	6.15E–11	6.28E–18
74b27p23	50	0.076	0.0011	0.005	8.33E–11	7.35E–08	174.46	17.78	234.00	3.14E–10	3.20E–17
74b27p17	50	0.076	0.0011	0.011	1.83E–10	1.62E–07	167.41	17.07	224.54	7.20E–10	7.34E–17
74b27p18	50	0.076	0.0011	0.031	5.17E–10	4.56E–07	158.29	16.14	212.31	2.15E–09	2.19E–16
74b27p19	50	0.076	0.0011	0.051	8.50E–10	7.49E–07	168.45	17.17	225.94	3.32E–09	3.38E–16
74b27p20	50	0.076	0.0011	0.071	1.18E–09	1.04E–06	167.75	17.10	225.00	4.64E–09	4.73E–16
74b27p21	50	0.076	0.0011	0.091	1.52E–09	1.34E–06	167.29	17.05	224.38	5.96E–09	6.08E–16

Table T5. Permeability test results for Sample 190-1174B-33R-4, 20–35 cm (452.90 mbsf), trimmed at 21.5–29.1 cm.

Sample and test number	Effective pressure (kPa)	Length (m)	Area (m^2)	Flow rate (mL/min)	Flow rate (m^3/s)	Fluid flux (m/s)	Differential pressure (kPa)	Head (m)	Head gradient (m)	Hydraulic conductivity (m/s)	Intrinsic permeability (m^2)
Adat01	50	0.076	0.0011	0.005	8.33E–11	7.35E–08	13.48	1.37	18.08	4.06E–09	4.15E–16
Adat02	100	0.076	0.0011	0.005	8.33E–11	7.35E–08	59.38	6.05	79.64	9.23E–10	9.41E–17
Adat03	150	0.076	0.0011	0.005	8.33E–11	7.35E–08	107.03	10.91	143.56	5.12E–10	5.22E–17
Adat04	250	0.076	0.0011	0.005	8.33E–11	7.35E–08	210.94	21.50	282.93	2.60E–10	2.65E–17
Adat05	350	0.076	0.0011	0.005	8.33E–11	7.35E–08	312.70	31.88	419.42	1.75E–10	1.79E–17
Adat06	350	0.076	0.0011	0.011	1.83E–10	1.62E–07	311.91	31.80	418.36	3.86E–10	3.94E–17
Adat07	350	0.076	0.0011	0.000501	8.35E–12	7.36E–09	212.30	21.64	284.75	2.59E–11	2.64E–18
Adat08	350	0.076	0.0011	0.000025	4.17E–13	3.67E–10	12.91	1.32	17.32	2.12E–11	2.16E–18
Adat09	450	0.076	0.0011	0.000025	4.17E–13	3.67E–10	16.16	1.65	21.67	1.70E–11	1.73E–18
Adat10	450	0.076	0.0011	0.000501	8.35E–12	7.36E–09	222.07	22.64	297.86	2.47E–11	2.52E–18
Adat11	550	0.076	0.0011	0.000501	8.35E–12	7.36E–09	257.62	26.26	345.54	2.13E–11	2.17E–18
Adat12	550	0.076	0.0011	0.000025	4.17E–13	3.67E–10	26.95	2.75	36.15	1.02E–11	1.04E–18